i2Nav-Robot: A Large-Scale Indoor-Outdoor Robot Dataset for Multi-Sensor Fusion Navigation and Mapping

Hailiang Tang, Tisheng Zhang, *IEEE Member*, Liqiang Wang, Xin Ding, Man Yuan, Zhiyu Xiang, Jujin Chen, Yuhan Bian, Shuangyan Liu, Yuqing Wang, Guan Wang, and Xiaoji Niu, *IEEE Member*

Abstract—Accurate and reliable navigation is crucial for autonomous unmanned ground vehicle (UGV). However, current UGV datasets fall short in meeting the demands for advancing navigation and mapping techniques due to limitations in sensor configuration, time synchronization, ground truth, and scenario diversity. To address these challenges, we present i2Nav-Robot, a large-scale dataset designed for multi-sensor fusion navigation and mapping in indoor-outdoor environments. We integrate multi-modal sensors, including the newest front-view and 360-degree solid-state LiDARs, 4-dimensional (4D) radar, stereo cameras, odometer, global navigation satellite system (GNSS) receiver, and inertial measurement units (IMU) on an omnidirectional wheeled robot. Accurate timestamps are obtained through both online hardware synchronization and offline calibration for all sensors. The dataset includes ten larger-scale sequences covering diverse UGV operating scenarios, such as outdoor streets, and indoor parking lots, with a total length of about 17060 meters. High-frequency ground truth, with centimeter-level accuracy for position, is derived from post-processing integrated navigation methods using a navigation-grade IMU. The proposed i2Nav-Robot dataset is evaluated by more than ten open-sourced multi-sensor fusion systems, and it has proven to have superior data quality.

Index Terms—UGV dataset, navigation and mapping dataset, multi-sensor fusion navigation, positioning and mapping.

I. INTRODUCTION

UNMANNED ground vehicle (UGV) is a kind of robot in contact with the ground, such as indoor buildings and outdoor roads. Nowadays, the UGV has been widely employed for intelligent transportation applications, such as logistics, cleaning, and patrol, especially with the rapid development of artificial intelligence. As the foundation of perception, planning,

The authors are with the Intelligent and Integrated Navigation Group (i2Nav), GNSS Research Center, Wuhan University, Wuhan 430079, China. (e-mail: thl@whu.edu.cn; zts@whu.edu.cn; wlq@whu.edu.cn; dingxin@whu.eud.cn; yuanman@whu.edu.cn; xiangzy@whu.edu.cn; chenjujin@whu.edu.cn; yuhanbian@whu.edu.cn; liushuangyan@whu.edu.cn; wyq_slam@whu.edu.cn; wanguan@whu.edu.cn; xjniu@whu.edu.cn).

Hailiang Tang, Tisheng Zhang, and Xiaoji Niu, are also with the Hubei Technology Innovation Center for Spatiotemporal Information and Positioning Navigation, Wuhan 430079, China, and the Hubei Luojia Laboratory, Wuhan 430079, China.

The i2Nav-Robot dataset together with the documents and calibration files can be accessed on GitHub (https://github.com/i2Nav-WHU/i2Nav-Robot).

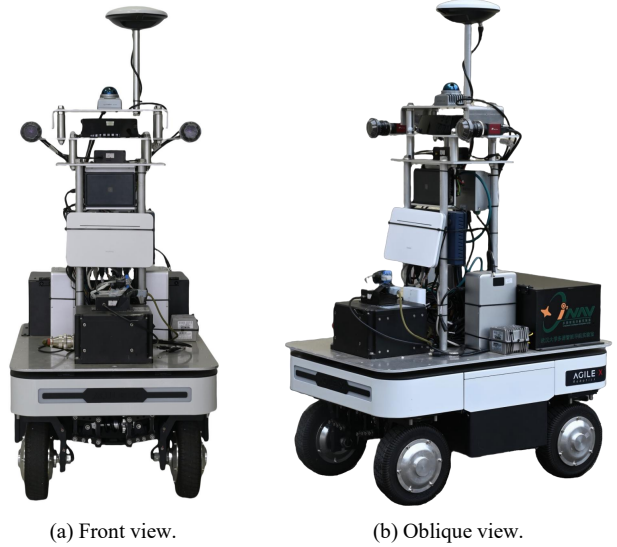(a) Front view. (b) Oblique view.

Fig. 1. The omnidirectional robot employed in the i2Nav-Robot dataset.

and control [1], accurate and reliable position and attitude are of great importance for autonomous UGV applications. The global navigation satellite system/inertial navigation system (GNSS/INS) integrated system [2], [3], as a classical method, has already become a basic part of UGVs. For civil applications, the intelligent UGV usually works in closed environments, such as campus, park, and residential district. In such complex environments, the GNSS signals may be interfered, decayed, and even interrupted, and thus the navigation accuracy may be degraded [4]. Due to time-varying biases of the low-cost inertial measurement unit (IMU), extra information should be adopted to mitigate the INS drift in GNSS-denied environments.
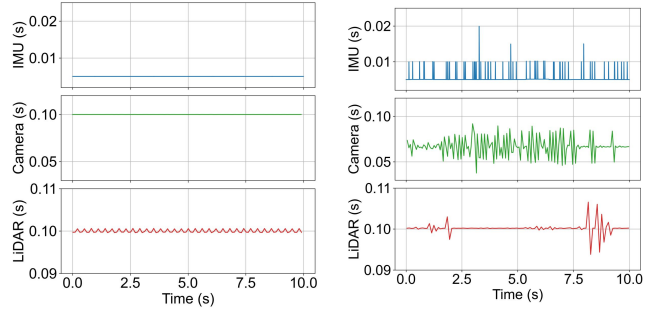
Different from unmanned aerial vehicles (UAV) and unmanned surface vehicles (USV), the wheeled UGV is usually equipped with a low-cost odometer (ODO) on each wheel [5], and we can obtain precise wheel speed from the ODO [6]. By incorporating the wheel speed and optional wheel angle from the ODO, the INS drifts can be reduced notably in a GNSS/INS/ODO integration system [7], [8]. Nevertheless, the navigation accuracy still cannot be guaranteed in environments with long-term GNSS interruptions, such as urban canyons and indoor parking lots. Thus, the LiDAR and visual simultaneous localization and mapping (SLAM) methods [9], [10] should be employed to enhance the reliability and robustness. As a result, a multi-sensor fusion navigation system can be constructed, and

it is a practical and reliable solution for autonomous UGV applications. However, current UGV datasets have been unable to meet the demand of advancing navigation and mapping, especially when the newest solid-state LiDARs and 4-dimensional (4D) millimeter-wave (MMW) radars have been equipped in newly mass-produced UGVs.

In terms of sensor configurations, a GNSS receiver, a micro-electro-mechanical systems (MEMS) IMU, and several ODOs have already been the standard components of commercial wheeled UGVs. This is because GNSS/INS/ODO integration can complete most navigation tasks on larger-scale outdoor roads, which are the common application scenarios for a UGV. The ODO is a low-cost and precise sensor, but the M2DGR [11] dataset does not contain an ODO. Some datasets, such as OpenLORIS-Scene [12], Kimera-Multi [13], and BotanicGarden [14], mainly focus on SLAM methods, and they do not contain the GNSS receiver. Hence, these datasets without GNSS are not very suitable for large-scale multi-sensor navigation. Vision sensors or RGB cameras have been almost used in all UGV datasets, due to the lower cost and comparable accuracy. Besides, multiple cameras are commonly equipped to increase the field of view (FOV), and the stereo camera system has become the most popular and practical configuration for navigation applications.

Unlike vision sensors, the 3D LiDAR can conduct distance measurement directly, and it can achieve more robust and accurate navigation. Besides, the 3D LiDAR can also be used to build a point-cloud map, which can be further employed for map-matching-based navigation. Nevertheless, there is no LiDAR in the Rosario [15] dataset. Besides, the LiDAR sensor has been developed rapidly in the past decade, and the conventional spinning LiDAR has been gradually replaced by newly (half)-solid-state LiDARs. For example, the M3DGR [16] dataset employs a Livox AVIA front-view LiDAR and a Livox Mid360 360-degree LiDAR, which are all solid-state LiDARs. Recently, a kind of solid-state automotive-grade LiDAR with the horizontal FOV of about 120° and the vertical FOV of about 25°, such as the RoboSense M1 and Hesai AT128, has been applied in the newly autonomous vehicles and UGVs. However, such solid-state LiDARs have not yet been adopted in the current UGV datasets. Like solid-state LiDARs, the 4D millimeter-wave radar has already been equipped in recent autonomous UGVs for robust perception under extreme environments. The 4D radar can be employed as a supplement for environment perception by outputting object-detection results, and it can also provide can provide raw distance, evaluation angle, azimuth angle, and Doppler velocity [17] these 4D data. So far, the 4D radar has been contained in some vehicle or handheld datasets, such as EU Long-term [18] and NTU4DRadLM [19], but not in current UGV datasets. Hence, there is a large gap between the current UGV datasets and the mass-produced UGVs, in terms of the LiDAR and 4D radar.

When multiple heterogeneous sensors, including GNSS, MEMS IMU, camera, LiDAR, and 4D radar, are installed in the same UGV, the time synchronization becomes a complex problem. This is because that different sensor data is asynchronously obtained from different interfaces, such as the

(a) Hardware synchronization.　　(b) Software synchronization.

Fig. 2. Comparison of the intervals of sensors' timestamps. The intervals obtained from the hardware synchronization are much steadier than that of the software synchronization, which usually means more accurate synchronization.

universal serial bus (USB) port, serial port, and Ethernet port. A naive solution is to stamp the receiving time on the host computer to the sensor data, and this is called software synchronization. Datasets like NCLT [20], Rosario [15], M2DGR [11], and M3DGR [16] all employ software synchronization. However, the software synchronization is inaccurate, and this may cause large errors and reduce the navigation reliability. In M2DGR [11], the authors claim that they achieve a software synchronization of less than 10 ms. However, a time error of 10 ms will result in an angle error of 0.5° when the angular velocity is 50 °/s, which is a normal value for a wheeled UGV. For this reason, NCLT [20] and OpenLORIS-Scene [12] datasets try to calibrate the time offsets caused by software synchronization. However, the unstable time intervals of sensor data cannot be calibrated, and this may introduce larger errors for navigation and mapping, as shown in Fig. 2. The hardware synchronization using embedded triggers can achieve a microsecond-level synchronization accuracy, and it has been employed in many datasets, such as FusionPortable [21], FusionPortableV2 [22], and MARS-LVIG [23]. Meanwhile, the precision time protocol (PTP) can also be used to synchronize different sensors though an Ethernet interface, and it almost achieves the same accuracy as the trigger-based synchronization. PTP has been supported by recent LiDARs and cameras, and the data acquisition and time synchronization can be completed simultaneously through one single Ethernet port. As a result, the trigger-based and PTP-based hardware synchronization can be utilized together for accurate time synchronization, such as in BotanicGarden [14] dataset.

Ground truth is another critical part for a practical dataset. For outdoor environments, GNSS real-time kinematic (RTK) with a centimeter-level accuracy can be adopted as ground-truth positions, such as in Rosario [15] and M3DGR [16] datasets. However, the GNSS RTK usually has a very low data rate, which is not enough for a complete evaluation. Besides, the ground-truth attitudes cannot be obtained with only one GNSS antenna. Hence, the low-cost GNSS/INS integration, which can provide both positions and attitudes, is employed as the ground-truth system in FusionPortableV2 [22], but the ground-truth pose is absent in GNSS-denied environments. The NCLT [20] dataset employs both the GNSS

TABLE I
COMPARISON OF THE OPEN-SOURCED UGV DATASETS

Dataset, Year	Overview				Sensors					Ground truth			Scenarios[6]		
	UGV[1]	Sync.[2]	All in one[3]	Large scale[4]	Vision	Front-view LiDAR	360-degree LiDAR	4D Radar	ODO[5]	Pose	Velocity	Rate (Hz)	IN	OUT	IO
NCLT, 2016	Two-wheel Segway	Software		●	●		●		Pose	●		100		●	●
Rosario, 2019	Four-wheel Ackerman	Software	●		●				●	Position Only		5		●	
M2DGR, 2022	Four-wheel Ackerman	Software	●		●	RGB-D	●			●		10~100	●	●	●
FusionPortableV2 (UGV), 2024	Four-wheel Ackerman	Hardware	●		●		●		●	●		30		●	
M3DGR, 2025	Four-wheel Ackerman	Software	●		●	●	●		●	Half[7]		5	●	●	
i2Nav-Robot (ours), 2025	Four-wheel omnidirectional	Hybrid[8]	●	●	●	●	●	●	●	●	●	200	●	●	●

[1]The UGV type. [2]The time-synchronization mode for different sensors. [3]All sensors' data for each sequence is contained in a single file, typically the ROS bag file. [4]Datasets with every sequence longer than one kilometer are defined as large-scale datasets. [5]The odometer (ODO) denotes the wheel speeds and optional wheel angles. [6]IN is indoor; OUT is outdoor; IO denotes that there are both indoor and outdoor environments in a single sequence. [7]There are ground-truth poses for indoor sequences from Mocap, while only positions for outdoor sequences from GNSS. [8]Using hardware synchronization for supported sensors, otherwise using software synchronization with offline calibrations.

RTK and LiDAR SLAM to generate ground-truth poses for indoor-outdoor environments, but the pose accuracy cannot be guaranteed in large-scale indoor environments. The motion capture (Mocap) system has been a common ground-truth system for indoor environments, and the pose rate can be more than 100 Hz. For example, the famous EuRoC UAV [24] datasets, and M2DGR [11] and M3DGR [16] datasets all use the Mocap as the ground-truth system. Nevertheless, the Mocap is only suitable for an indoor laboratory or a certain region because the working region of the Mocap is limited by the expensive high-speed camera. Hence, it is challenging to generate reliable ground-truth poses in large-scale indoor environments, which limits the testing environments of the current datasets. Meanwhile, most of the current datasets do not provide ground-truth velocity, which can be employed for many usages, such as accuracy evaluation and time calibration.

Overall, the existing UGV datasets have exhibited some deficiencies in sensor configuration, time synchronization, ground truth, and scenario diversity, as shown in Table I. As UGVs with new sensors have gradually entered the commercial operation stage, current datasets can no longer meet the needs of modern navigation and mapping methods. Hence, the Intelligent and Integrated Navigation Group (i2Nav) from Wuhan University presents the i2Nav-Robot dataset with multi-modal sensors, accurate time synchronization, reliable ground truth, and abundant application scenarios for UGVs. Fig. 1 shows the four-wheel omnidirectional robot adopted in the i2Nav-Robot dataset. The main contributions of our work are as follows:

● Multi-modal sensors, including front-view solid-state LiDAR, 360-degree solid-state LiDAR, 4D MMW radar, stereo cameras, GNSS receivers, IMU, and wheeled ODO, are well integrated on an omnidirectional robot, enabling complete motion perception for accurate navigation and mapping.

● Both the trigger-based and PTP-based hardware synchronizations are employed to obtain accurate timestamps for nearly all sensors, which ensures the higher quality of the proposed dataset. Besides, the fixed time offsets for the software-synchronized radar and ODO are calibrated offline using a speed-based method.

● Ten large-scale sequences with a total length of more than 17000 meters and 14000 seconds are collected in diverse environments, such as outdoor streets, indoor parking lots, and indoor-outdoor buildings, which are all potential application scenarios for a commercial UGV.

● A navigation-grade IMU is adopted to provide high-frequency ground-truth position, attitude, and velocity for all sequences. The post-processing GNSS/INS integration is adopted to derive centimeter-level ground truth for outdoor sequences, and the post-processing map-matching (MM)/INS integration is used for GNSS-challenging sequences.

● The proposed dataset is examined by more than ten open-sourced odometry and GNSS-based systems. Sufficient results demonstrate the extraordinary data quality of the i2Nav-Robot dataset. Besides, experiment results show that the sensors are well synchronized, and the provided calibration parameters are exactly accurate.

In the following sections, we first give an overview of the i2Nav-Robot dataset. In Section III, the details of the ground-truth system are presented. Then, the dataset descriptions are introduced in Section IV. Experiments and results for quantitative evaluation are discussed in Section V. Finally, we make a brief conclusion of the presented i2Nav-Robot dataset.

II. SYSTEM OVERVIEW

A. Sensor Setup

The multi-sensor robot employed in i2Nav-Robot dataset is built upon a four-wheel omnidirectional robot, *i.e.,* AgileX Ranger Mini3, as shown in Fig. 1 and Fig. 3. A Jetson AGX Orin board from NVIDIA is employed to collect all sensor data through the Robot Operating System (ROS). The Ranger chassis can output wheel speeds and wheel angles from the four
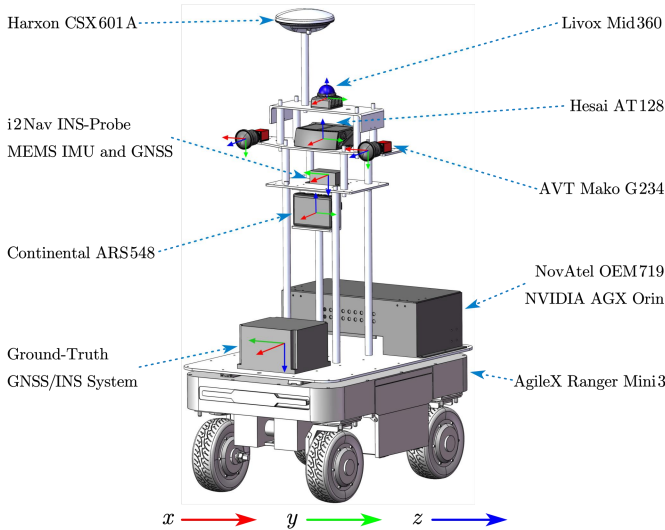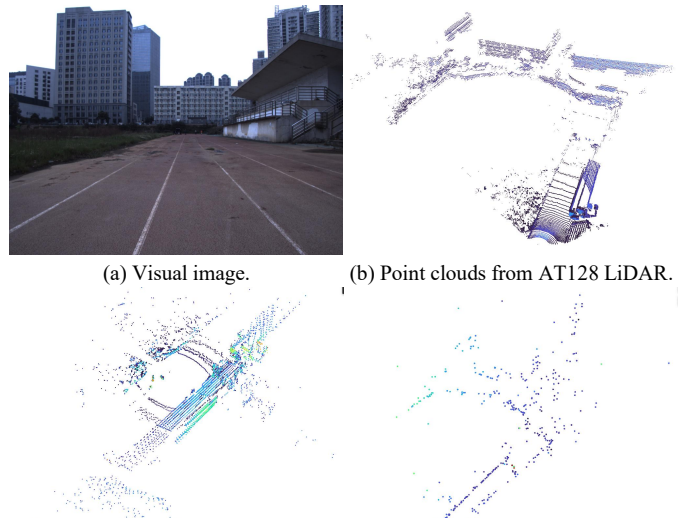
Fig. 3. The 3D model of the robot together with the coordinate frames.

(a) Visual image. (b) Point clouds from AT128 LiDAR.

(c) Point clouds from Mid360 LiDAR. (d) Point clouds from ARS548 radar.

Fig. 4. Multi-modal perception from vision, front-view LiDAR (AT128), 360-degree LiDAR (Mid-360), and 4D radar.
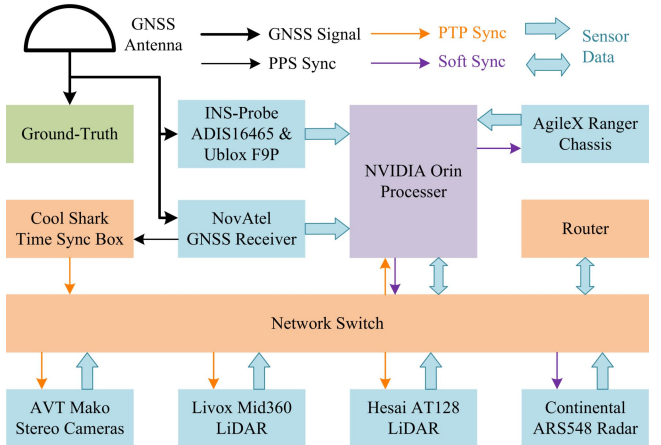
TABLE II
THE EQUIPPED SENSORS AND SPECIFICATIONS

Sensor	Type	Characteristic
ADI ADIS16465	IMU	In-run bias stability: 2 °/hr Angular random walk: 0.15 °/√hr
Ublox F9P	GNSS	Multi-system supported L1/L2 double frequency
Harxon CSX601A	GNSS antenna	Full GNSS frequency supported
NovAtel OEM719	GNSS	Multi-system and multi-frequency supported
AVT Mako-G234 (Stereo)	Camera	Global shutter and color mode Resolution: 1600*1200
Livox Mid360 (Built-in ICM40609)	360-degree LiDAR	Scanning line: 6 Horizontal: 360°, vertical: -7°~52° Range: 0.1~40 m @ 10% reflectivity
TDK ICM40609	IMU	Gyroscope noise: 4.5 mdps/ √ Hz Accelerometer noise: 100 ug/ √ Hz
Hesai AT128	Front-view LiDAR	Scanning line: 128 Horizontal: 120°, vertical: -12.5°~12.9° Range: 1~180 m @ 10% reflectivity
Continental ARS548	4D Radar	Horizontal: 120°, vertical: -20°~20° Range: 0.2~300 m, accuracy: ±0.15 m Speed accuracy: 0.1 m/s
AgileX Ranger Mini3	Odometer	Speed resolution: 0.001 m/s Angle resolution: 0.001 rad

Fig. 5. Time-synchronization flow.

wheels to the Orin through a Controller Area Network (CAN) bus. INS-Probe, a compact GNSS/INS integrated system from the i2Nav group, provides the IMU data from ADI ADIS16465 and the GNSS data from Ublox F9P. We also equipped a NovAtel OEM719 receiver to derive GNSS-RTK positioning results and raw observations. The INS-Probe and OEM719 are connected to the Orin through USB ports. The ground-truth GNSS/INS system includes a navigation-grade IMU with a gyroscope bias stability of 0.03 °/hr, which is used to generate the ground truth by integrating with the post-processing RTK or MM results. The GNSS signals for INS-Probe, OEM719, and ground-truth system are derived from a full-frequency antenna, *i.e.,* Harxon CSX601A, through a multi-port splitter.

Multi-modal perception sensors, including stereo cameras Mako-G234 from AVT, front-view solid-state LiDAR AT128 from Hesai, 360-degree solid-state LiDAR Mid360 from Livox,

and 4D MMW radar ARS548 from Continental, are installed on the robot using our self-designed mechanical structure. Particularly, the AT128 has a horizontal FOV of 120° and a vertical FOV of 25°, and this kind of LiDAR has become a substitute for conventional 360-degree spinning LiDARs in mass-produced UGVs. Meanwhile, the ARS5488 is a new 4D MMW radar, which can provide detected objects, such as pedestrians and vehicles. The ARS5488 can also provide point clouds and Doppler velocity measurements, which may be particularly useful for robust navigation, especially in visual and LiDAR degraded environments. Fig. 4 depicts the multi-modal perception from vision, front-view LiDAR, 360-degree LiDAR, and 4D radar. By fully using these perception sensors, we can achieve reliable and accurate multi-sensor fusion navigation and mapping in complex environments.

B. Time Synchronization

GNSS is the source of time for all the systems, as shown in Fig. 5. Cool Shark box is a module for PTP-based time synchronization. The ground-truth system, INS-Probe, and

Cool Shark box can maintain accurate clocks with their built-in crystal oscillators, even in GNSS-denied indoor environments. Besides, the ADIS16465 IMU in INS-Probe is synchronized through hardware trigger. Meanwhile, the Cool Shark box is the main clock for PTP through a local network switch. Hence, the cameras, LiDARs, and NVIDIA Orin can be synchronized to the GNSS time using PTP. These sensors synchronized through hardware can have microsecond-level timestamps. Note that the timestamps for stereo cameras correspond to the start time of exposure, and thus the exposure durations are not considered.

The ARS548 radar and AgileX ODO are synchronized using the system time on Orin when receiving the data, because they do not have a hardware-synchronization interface. Nevertheless, they are also precisely synchronized, as the NVIDIA Orin has been synchronized through PTP. Besides, the fixed time offsets for radar and odometer data can be calibrated offline.

C. Calibration

1) Calibration of Intrinsic and Extrinsic Parameters

The intrinsic and extrinsic parameters are important for accurate navigation and mapping. In the i2Nav-Robot dataset, the stereo cameras are modeled using the pinhole camera and radial-tangential distortion models [25]. The intrinsic and extrinsic parameters for stereo cameras are calibrated using MATLAB 2024b with an AprilTag [26] calibration board. The translation parts of the extrinsic parameters for all sensors are directly obtained from their 3D models, as exhibited in Fig. 3. We do not calibrate the rotation parts of the extrinsic parameter, as we think algorithms should have the capability to estimate and calibrate these parameters online. Nevertheless, we provide the LiDAR-IMU and camera-IMU extrinsic parameters estimated by the open-sourced FF-LINS [27] and LE-VINS [28], which are online available[1]. Besides, experiments are conducted to verify the accuracy of the provided extrinsic parameters in Section V.C.

2) Calibration of Time Offsets

The 4D radar and ODO they are synchronized through software, due to the lack of hardware-synchronization interface. Nevertheless, we employ a speed-based method to calibrate the fixed time offsets and improve the accuracy of time synchronization. For the ODO, the wheel speed and angle for the four-wheel omnidirectional robot can be expressed as v_i and α_i, where $i \in [1,4]$, and the ODO speed v_{ODO} can be written as

$$v_x = \sum_{i=1}^{4} v_i * \cos \alpha_i \tag{1}$$

$$v_y = \sum_{i=1}^{4} v_i * \sin \alpha_i \tag{2}$$

$$v_{ODO} = \sqrt{v_x^2 + v_y^2} \tag{3}$$

The v_x and v_y denote the forward and lateral speed, respectively, and v_y is almost equal to zero due to the dynamic
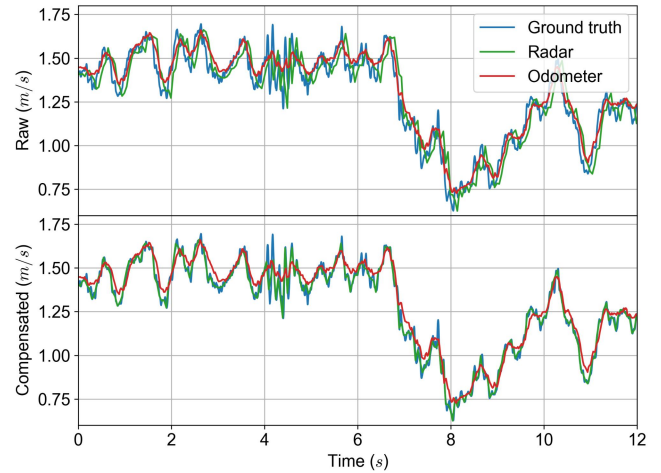
[1]https://github.com/i2Nav-WHU

Fig. 6. Comparison of the speeds before (Raw) and after (Compensated) compensating the fixed time offsets for radar and odometer. The ODO and radar are originally delayed, as shown in the top figure.

model of the omnidirectional robot [7]. For the 4D radar, we can obtain hundreds of points $\boldsymbol{p}_{R,j}$ with Doppler speeds $v_{R,j}$, where j is the point index. Hence, we can estimate the radar velocity $\boldsymbol{v}_R$ by solving the following least-square problem as

$$arg \min_{\boldsymbol{v}_R} \sum_j \left\| \boldsymbol{v}_R^T \cdot \boldsymbol{u}_{R,j} - v_{R,j} \right\|^2 \tag{4}$$

where $\boldsymbol{u}_{R,j} = \boldsymbol{p}_{R,j} / \|\boldsymbol{p}_{R,j}\|$ is the direction vector of $\boldsymbol{p}_{R,j}$. The radar speed v_{Radar} is the norm of the radar velocity $\boldsymbol{v}_R$.

As a result, we can derive the time series of the ODO and radar speed. The fixed time offsets can be estimated by conducting a cross-correlation analysis with the ground-truth speed series. The raw ground-truth speed with a rate of 200 Hz is interpolated into 1000 Hz, to obtain an estimation accuracy of about 1.0 ms. According to our experiments, the fixed time offset for the ODO is about -10 ms, while about -100 ms for radar, mainly because the amount of radar data is much larger. The negative signs denote that the ODO and radar data are delayed. As depicted in Fig. 6, the radar and ODO speeds are synchronized to the ground truth speed after compensating for the time offsets. Hence, the radar and ODO can also achieve an accuracy of 1.0 ms, which is much better than the uncalibrated software synchronization.

III. GROUND-TRUTH SYSTEM

A navigation-grade IMU is employed as the ground-truth system, which can provide high-frequency (200 Hz) positions with centimeter-level accuracy, attitudes, and velocities. For sequences with good GNSS observations, we employ a tightly-coupled GNSS/INS integration to generate the ground truth, otherwise use a loosely-coupled MM/INS integration.

A. GNSS/INS Integration

The GNSS raw observations from OEM719 receiver, including pseudorange, carrier phase, and Doppler, are collected for post-processing GNSS/INS integrated navigation. The commercial software Inertial Explorer (IE) from NovAtel is adopted to process the GNSS data from OEM719 and IMU data from the navigation-grade IMU. Besides, the IMU-rate
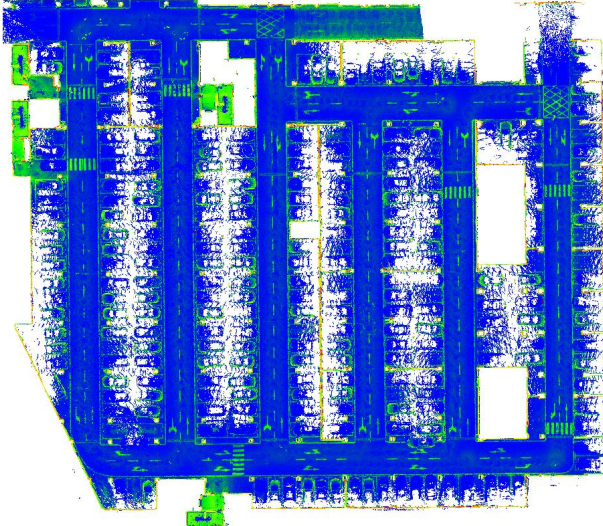
Fig. 7. The prebuilt point-cloud map of the second floor in the parking lot (used by three parking sequences). The traffic lines are clear to distinguish, which demonstrates the high quality of the map. This map has been cut for better visualization.
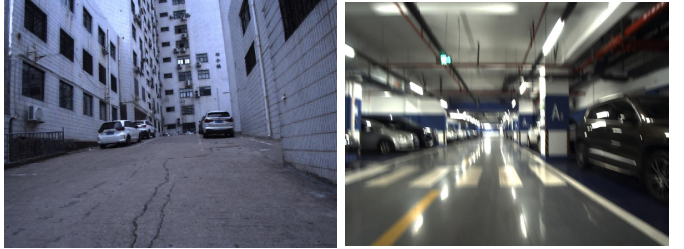

Fig. 8. Sequences overview in the i2Nav-Robot dataset. Each color denotes a different sequence.

(200 Hz) ground-truth positions, attitudes, and velocities are derived from the combined solution in IE, and thus they are all smoothed with higher accuracy.

B. MM/INS Integration

In GNSS-challenging urban canyons or GNSS-denied indoor parking lots, we cannot obtain centimeter-level RTK results, and the GNSS/INS integration may be unreliable in such scenarios. Hence, we employ an MM-based method to derive accurate ground truth in GNSS-denied environments. Specifically, we first build large-scale point-cloud maps in the building and parking scenarios, using a commercial LiDAR SLAM system, *i.e.*, the RS100i-MT from GoSLAM. Meanwhile, the built maps are aligned to the geodetic coordinate by incorporating several RTK control points. Next, we use a multi-sensor fusion method with MM-based constraints from the AT128 LiDAR to obtain coarse position results and distortion-removed point clouds. Then, an optimization-based method is employed to derive the independent MM results using the point clouds from AT128 and the prebuilt point-cloud map. Finally, the MM positions and the navigation-grade IMU are integrated by our self-developed post-processing software. As a result, we can

(a) GNSS-degenerated urban canyon.

(b) Motion blur.

(c) Structureless scene.

(d) Dynamic objects.

Fig. 9. Challenges for different sensors. (a) shows the GNSS-challenging environments. (b) shows the motion blur of camera. (c) shows a structureless scene for LiDAR and radar. (d) is a dynamic environment, which is challenging for perception sensors.

TABLE III
THE SEQUENCE DETAILS

Sequence	Duration (s)	Trajectory (m)	Scene[1]	Challenges	GT
building00	1201	1673	OUT	GNSS degenerated	MM/INS
building01	1369	1730	IO	Illumination	MM/INS
building02	2110	2522	OUT	Dynamic	GNSS/INS
parking00	1141	1583	IO	Illumination	MM/INS
parking01	1060	1224	IN	Motion blur	MM/INS
parking02	1257	1442	IN	Motion blur	MM/INS
playground00	1786	1711	OUT	Structureless	GNSS/INS
street00	1380	1668	OUT	Dynamic	GNSS/INS
street01	1520	1660	OUT	Dynamic	GNSS/INS
street02	1380	1847	OUT	Dynamic	GNSS/INS
Total	14204	17060	-	-	-

[1]IN denotes indoor; OUT denotes outdoor; IO denotes indoor and outdoor.

obtain centimeter-level ground truth positions even in GNSS-denied scenarios. Fig 7 exhibits the prebuilt point-cloud map of the second floor in the parking lot. The traffic lines are clear to distinguish, demonstrating the high quality of the map.

IV. DATASET DESCRIPTION

A. Sequence Characteristics

The i2Nav-Robot dataset was collected in diverse scenarios in the campus of Wuhan University, which are the typical application scenarios for a commercial logistics and cleaning UGVs. Specifically, we collected ten sequences, including *building*, *playground*, *parking*, and *street* sequences. Fig. 8 shows the trajectories and scenarios of these ten sequences.

Table III shows the details about the ten sequences, and the total trajectory length is about 14204 seconds and 17060 meters. The MM/INS integration is employed to derive the ground truth in building and parking scenarios, as shown in Table III. Besides, both indoor, outdoor, and indoor-outdoor sequences

TABLE V
THE ABSOLUTE ERRORS FOR ODOMETRY SYSTEMS

ARE (°) / ATE (m)	VINS-Mono	OpenVINS (Stereo)	DM-VIO	DLIO	FF-LINS	FAST-LIO2	FAST-LIVO2	LE-VINS	R3LIVE
building00	0.48 / 3.95	1.34 / 3.36	0.52 / 2.45	0.90 / **0.39**	2.19 / 2.32	1.20 / 0.68	0.91 / 1.10	**0.39** / 1.17	Failed
building01	0.74 / 2.74	0.86 / 1.13	0.76 / 2.42	0.86 / 0.43	1.35 / 1.16	0.93 / 0.38	0.43 / **0.19**	**0.36** / 1.01	Failed
building02	1.21 / 6.51	0.34 / 1.48	**0.34** / 10.31	8.56 / 9.62	2.82 / 6.73	0.76 / **1.46**	1.04 / 1.65	0.79 / 2.35	1.70 / 4.49
parking00	1.14 / 7.53	**0.33** / 0.88	0.37 / 1.19	0.73 / 0.46	2.48 / 1.94	0.45 / **0.25**	0.56 / 0.26	0.50 / 0.98	1.12 / 0.59
parking01	3.67 / 3.86	0.34 / 0.81	0.83 / 2.33	0.58 / 0.15	1.69 / 1.06	1.21 / 0.44	0.65 / **0.17**	**0.30** / 0.69	0.91 / 0.39
parking02	3.13 / 3.24	2.34 / 3.47	0.85 / 1.31	1.08 / 0.56	1.64 / 1.31	2.07 / 1.46	**0.65** / **0.18**	0.69 / 0.79	1.37 / 0.66
playground00	0.51 / 2.59	0.92 / 1.62	0.85 / 8.07	8.21 / 0.44	1.43 / 1.71	**0.41** / **0.31**	0.49 / 0.53	0.84 / 1.34	0.52 / 0.62
street00	0.57 / 3.81	0.84 / 1.60	Failed	0.73 / **0.79**	2.22 / 3.32	1.38 / 1.86	0.81 / 1.12	**0.53** / 1.18	1.34 / 1.61
street01	1.07 / 8.71	0.37 / **1.11**	0.64 / 3.44	8.84 / 4.31	1.75 / 4.20	0.72 / 1.28	1.15 / 2.45	**0.34** / 1.65	1.43 / 2.36
street02	0.83 / 6.72	**0.46** / 1.61	1.35 / 7.43	1.39 / 3.15	1.95 / 3.78	0.91 / 1.49	1.19 / 2.92	0.51 / 2.16	1.32 / **1.40**
RMS	1.71 / 5.38	1.01 / 1.93	Invalid	4.74 / 3.50	2.00 / 3.23	1.11 / **1.12**	0.83 / 1.42	**0.55** / 1.43	Invalid

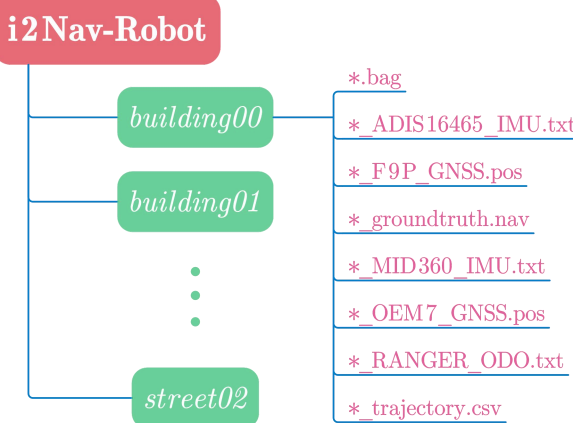The bold result denotes the best among these systems.

Fig. 10. The dataset organization, where * denotes the sequence name. There are six or eight files in the directory of each sequence, and GNSS files are not included in indoor sequences.

TABLE IV
THE TOPICS DETAILS IN THE ROS BAG FILE

Topic	Rate (Hz)	Message Type
/adi/adis16465/imu	200	sensor_msgs::Imu
/insprobe/adis16465/imu	200	insprobe_msgs::Imu
/livox/mid360/imu	200	sensor_msgs::Imu
/ublox/f9p/fix	1	sensor_msgs::NavSatFix
/novatel/oem7/fix	1	sensor_msgs::NavSatFix
/avt_camera/left/image/compressed	10	sensor_msgs::CompressedImage
/avt_camera/right/image/compressed	10	sensor_msgs::CompressedImage
/livox/mid360/points	10	livox_ros_driver::CustomMsg
/hesai/at128/points	10	sensor_msgs::PointCloud2
/continental/ars548/detection	20	sensor_msgs::PointCloud2
/continental/ars548/object	20	sensor_msgs::PointCloud2
/insprobe/ranger/odometer	50	insprobe_msgs::Odometer

data format can be found in our online documents.

V. EXPERIMENTS

We conduct exhaustive experiments to evaluate the quality of the presented i2Nav-Robot dataset. More than ten odometry and GNSS-based systems are included for a comprehensive evaluation. Meanwhile, we also carry on experiments to verify the accuracy of spatial-temporal synchronization. The left camera, ADIS16465 IMU, AT128 LiDAR, and GNSS-RTK results from OEM719 are employed for experiments.

A. Evaluation of Odometry Systems

Odometry methods, such as visual-inertial odometry (VIO), LiDAR-inertial odometry (LIO), and LiDAR-visual-inertial odometry (LVIO), determine the navigation accuracy in GNSS-denied environments. Hence, the performance of an odometry is crucial for an autonomous UGV. Three state-of-the-art (SOTA) VIOs, including VINS-Mono [29], OpenVINS [30], and DM-VIO [31], and three LIOs, including DLIO [32], FF-LINS [27], and FAST-LIO2 [33], are adopted for evaluation. Meanwhile, three LVIOs using both camera and LiDAR, including FAST-LIVO2 [34], LE-VINS [28], and R3LIVE [35], are also included. The results of these nine odometry systems are exhibited in Table V. The absolute translation rotation error (ARE) and absolute translation error (ATE) are calculated using evo [36].

are included, which provides challenges for multi-sensor fusion navigation methods. Fig. 9 depicts several challenging scenes for different sensors, such as GNSS-degenerated urban canyon in the *building00* sequence and motion blur for cameras in the indoor parking sequences. Besides, the LiDAR and radar may be degenerated in structureless scenes of the *playground00* sequence, and the dynamic objects may impact the performance of all perception sensors. These challenges can be very meaningful to evaluate the robustness and reliability of a multi-sensor fusion method.

B. Data Format

We provide all-in-one ROS bag files for all sequences, and thus the users can examine the dataset at once. Table IV shows the topic information, including topic name, frame rate, and message type. We also provide raw text files for IMU, GNSS, and ODO data, which can be utilized for applications like GNSS/INS integration. Meanwhile, two types of ground truth files are included in the dataset. The "*_groundtruth.nav" file includes the high-frequency positions, attitudes, and velocities, and the "*_trajectory.csv" file contains the positions and attitude quaternions. The dataset organization is shown in Fig. 10, and the GNSS position files are not contained in the indoor sequences *parking01* and *parking02*. More details about the

TABLE VI
THE ABSOLUTE ERRORS FOR GNSS-BASED SYSTEMS

ARE (°) / ATE (m)	KF-GINS	OB-GINS	VINS-Fusion (Mono)	IC-GVINS	BA-GLINS
building00	66.08 / 13.91	1.66 / 8.46	36.60 / 14.04	**0.30** / 0.72	0.53 / **0.50**
building01	9.45 / 11.26	10.22 / 12.16	9.12 / 10.83	0.36 / 0.33	**0.26** / **0.17**
building02	1.75 / 2.72	1.37 / 2.80	8.27 / 2.80	0.23 / 0.23	**0.22** / **0.20**
parking00	34.16 / 23.28	24.75 / 23.87	24.20 / 23.25	**0.49** / 0.74	0.54 / **0.27**
playground00	0.56 / 0.40	1.17 / 0.40	9.40 / 0.31	**0.15** / **0.11**	0.23 / 0.12
street00	1.28 / 0.40	1.78 / 0.40	1.42 / 0.29	**0.15** / **0.10**	0.17 / 0.11
street01	1.20 / 0.48	1.06 / 0.48	0.89 / 0.29	0.46 / 0.29	**0.24** / **0.10**
street02	0.70 / 0.42	1.51 / 0.42	4.11 / 0.26	**0.19** / 0.12	0.33 / **0.12**
RMS	26.53 / 10.43	9.55 / 9.98	16.53 / 10.39	**0.32** / 0.41	0.34 / **0.24**

According to the results in Table V, only DM-VIO and R3LIVE fail to run on certain sequences, demonstrating the excellent quality of the dataset. Besides, the VIO OpenVINS, LIO FAST-LIO2, and LVIO FAST-LIVO2, can achieve the best results on different sequences, which means that these systems are all correctly configured. Overall, FAST-LIO2 shows the best results among these systems in terms of the root-mean-square (RMS) result.

B. Evaluation of GNSS-based Systems

GNSS is the key factor to achieve accurate navigation and mapping in large-scale environments. Hence, we also evaluate GNSS-based multi-sensor fusion systems on the i2Nav-Robot dataset, including KF-GINS [37], OB-GINS [2], VINS-Fusion [38], IC-GVINS [39], and BA-GLINS (BA-LINS with GNSS) [10]. KF-GINS and OB-GINS are both GNSS/INS integrated navigation methods. VINS-Fusion and IC-GVINS are GNSS-visual-inertial navigation methods. BA-GLINS is a GNSS-LiDAR-inertial navigation method with a kind of frame-to-frame LiDAR bundle adjustment (BA) [10]. Note that we failed to run some SOTA multi-sensor fusion methods due to complex configurations, such as MINS [40] and GICI-LIB [41], and thus their results are not included.

Table VI shows the absolute errors of these GNSS-based systems. The *building00* is a GNSS-degenerated sequence, and the GNSS RTK exhibit wrongly fixed positions, as shown in Fig. 11. Besides, the *building01* and *parking00* are all indoor-outdoor sequences, in which the RTK is interrupted for a long time. As a result, all systems show worse results on the three sequences. Nevertheless, BA-GLINS almost achieves a decimeter-level positioning accuracy, while a sub-meter accuracy for IC-GVINS. This is because they employ an effective outlier-culling method for RTK, while other systems use all RTK results despite outliers. Particularly, BA-GLINS yield the smallest RMS result, as the LiDAR is more precise than the vision sensor.

The results in Table VI also demonstrate the higher accuracy of the ground-truth pose, as the ATEs of BA-GLINS and IC-GVINS in some sequences are about 0.1 m. Note that the real-time RTK results from the OEM719 are employed for experiments. In contrast, the post-processing tightly-coupled GNSS/INS integration is adopted to derive the ground truth positions, which are far more accurate than the RTK results from the OEM719. Hence, a ATE of 0.1 m can reflect the
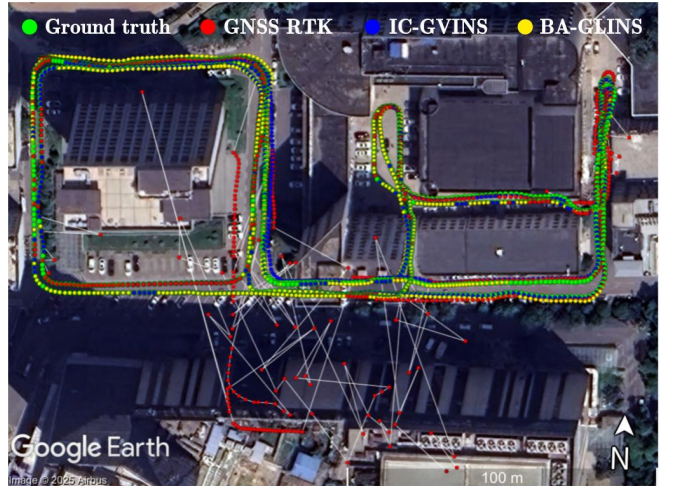

Fig. 11. Comparison of the results on the GNSS-degenerated sequence *builing00*. Due to the worse results, KF-GINS, OB-GINS, and VINS-Fusion are not included in this figure for better visualization.

higher accuracy of the ground-truth pose.

C. Evaluation of the Synchronization

The spatial-temporal synchronization is crucial for a multi-sensor fusion navigation or mapping system, especially for frequently used LiDAR, camera, and IMU sensors. The IMU can act as a converter of spatial-temporal parameters, and thus we evaluate the camera-IMU and LiDAR-IMU spatial-temporal synchronization to examine the dataset.

1) Camera-IMU Synchronization

The extrinsic parameters are not explicitly calibrated on the i2Nav-Robot dataset, as the navigation algorithm should adapt to the time-varying parameters, especially the rotation parameters. Hence, we provide the online estimated rotation parameters by LE-VINS (VIO mode) [28]. Table VII shows the results on each sequence, including the translation and rotation parts, and Fig. 12 shows the estimated parameters on the indoor-outdoor sequence *building01*.

The camera-IMU translation parameters obtained from the mechanical structure are (0.09, -0.2, -0.054), which is close to the results in Table VII. In terms of the mean value (0.087, -0.195, -0.042), the estimated translation parameters have an accuracy better than 2.0 cm. Meanwhile, both the translation and rotation parameters exhibit good consistency on different sequences, demonstrating the superior quality of the dataset. We notice the z-axis translation exhibits a large deviation on the *playground00*. This is because the ground is flat, lacking motion along the vertical axis, and thus this parameter is weakly observable. In short, results in Table VII show that the online estimated translation and rotation parameters have a repeatability of better than 2.0 cm and 0.1°, respectively, which demonstrates that the online calibrations can also yield a satisfactory accuracy.

We do not evaluate the time synchronization for camera and IMU on each sequence, due to the time-varying exposure time. Nevertheless, the estimated time-delay parameter by LE-VINS on the indoor-outdoor sequence *building01* is shown in Fig 12. Note that the camera-IMU time-delay parameter in LE-VINS is

<table>
<tr><th colspan="7">TABLE VII
ESTIMATED CAMERA-IMU EXTRINSIC PARAMETERS BY LE-VINS</th></tr>
</table>

Sequence	Translation (m)			Rotation (°)		
	x	y	z	x	y	z
building00	0.088	-0.195	-0.040	89.974	-0.184	89.663
building01	0.087	-0.195	-0.043	89.972	-0.177	89.700
building02	0.091	-0.195	-0.034	89.946	-0.171	89.694
parking00	0.091	-0.191	-0.036	89.936	-0.176	89.707
parking01	0.080	-0.178	-0.067	89.887	-0.171	89.679
parking02	0.082	-0.201	-0.059	89.870	-0.181	89.782
playground00	0.086	-0.199	***-0.018***	89.974	-0.187	89.667
street00	0.088	-0.202	-0.041	89.955	-0.172	89.677
street01	0.090	-0.194	-0.036	89.956	-0.175	89.711
street02	0.090	-0.202	-0.042	89.960	-0.168	89.684
Mean[1]	0.087 ±0.004	-0.195 ±0.007	-0.042 ±0.013	89.943 ±0.034	-0.176 ±0.006	89.696 ±0.032

[1]The mean value and the standard deviation. The estimated z-axis translation is much larger on the sequence *playground00* due to the weak observability.
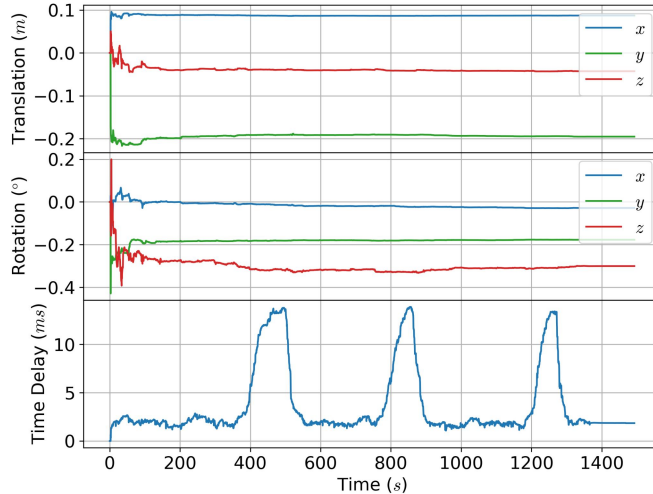

Fig. 12. Estimated camera-IMU extrinsic and time-delay parameters by LE-VINS on the indoor-outdoor sequence, *i.e.*, *building01*. Here, only the tiny rotation parameters are reserved for better visualization. The maximum exposure time for camera is set to 30 ms, and thus the estimated time-delay parameter is about 15 ms when in the indoor environments.

modeled as random walk, as it is time varying. According to our configurations, the maximum exposure time for camera is set to 30 ms, and thus the estimated time-delay parameter is about 15 ms (half of the exposure time) when in the indoor environments. As exhibited in Fig. 12, we can easily determine that the robot walks into the indoor parking lot three times, and LE-VINS can accurately estimate the exposure time with an accuracy of about one millisecond. The fixed time-delay parameter for camera and IMU in the outdoor environments is about 2.0 ms, due to the internal filters of ADIS16465. Nevertheless, the results demonstrate that the time-synchronization accuracy for camera and IMU is better than 1.0 ms.

2) LiDAR-IMU Synchronization

Similarly, we evaluate the LiDAR-IMU synchronization by analyzing the estimated extrinsic parameters by FF-LINS [27]. According to the mechanical structure, the LiDAR-IMU translation parameters are (0.042, -0.018, -0.063). As shown in Table VIII, the estimated translation error for x-axis and y-axis is within 1.0 cm, while 2.5 cm for z-axis. This is caused by the

<table>
<tr><th colspan="8">TABLE VIII
ESTIMATED LiDAR-IMU EXTRINSIC PARAMETERS BY FF-LINS</th></tr>
</table>

Sequence	Translation (m)			Rotation (°)			Time delay (ms)
	x	y	z	x	y	z	
building00	0.041	-0.014	-0.081	179.913	0.459	359.572	0.39
building01	0.038	-0.023	-0.099	179.918	0.407	359.543	0.20
building02	0.054	-0.022	-0.076	179.924	0.403	359.603	0.40
parking00	0.056	-0.022	-0.078	179.917	0.390	359.593	0.36
parking01	0.042	-0.018	-0.077	179.927	0.464	359.523	0.42
parking02	0.042	-0.02	-0.099	179.916	0.457	359.543	***0.84***
playground00	0.037	-0.009	***-0.161***	179.931	0.462	359.542	0.49
street00	0.049	-0.024	-0.091	179.902	0.448	359.609	0.39
street01	0.050	-0.021	-0.059	179.935	0.451	359.631	0.38
street02	0.055	-0.027	-0.061	179.927	0.449	359.569	0.56
Mean	0.046 ±0.007	-0.020 ±0.005	-0.088 ±0.028	179.921 ±0.009	0.439 ±0.026	359.573 ±0.034	0.44 ±0.16

The abnormal estimated time-delay parameter on the sequence *parking02* is caused by the drifts of crystal oscillators. Besides, the estimated z-axis translation is much larger on the sequence *playground00*, due to insufficient observability.

smaller FOV (25°) of the AT128 LiDAR in the vertical direction, and thus the z-axis translation is weakly observable. Meanwhile, the rotation parameters have a repeatability of about 0.1°. In short, the results in Table VIII illustrate that the provided extrinsic parameters have a higher accuracy.

The LiDAR and IMU sensors are accurately synchronized using hardware-based methods. According to the results in Table VIII, the mean value of the estimated time-delay parameter between LiDAR and IMU is about 0.44 ms. This tiny time may be caused by the internal processes of LiDAR and IMU. Besides, we notice the time-delay parameter is much larger on the sequence *parking02*. The three parking sequences are collected one by one, and thus the crystal oscillators may also drift when in the indoor environments without absolute time correction from the GNSS. Nevertheless, the LiDAR-IMU time synchronization has been proven to have an accuracy of about 1.0 ms.

VI. CONCLUSIONS

In this paper, we present a large-scale indoor-outdoor dataset i2Nav-Robot to satisfy the urgent need for high-quality UGV datasets. The newest front-view LiDAR, 360-degree LiDAR, and 4D MMW radar are utilized in the dataset to follow the development of the modern mass-produced autonomous UGVs. Besides, multiple sensors are precisely synchronized or calibrated to achieve a time-synchronization accuracy better than one millisecond. Ten large-scale sequences with a total length of more than 17 kilometers are collected in both indoor, outdoor, and indoor-outdoor scenarios. Meanwhile, the high-frequency and accurate ground-truth positions, attitudes, and velocities are provided for all sequences.

The i2Nav-Robot dataset is presented for autonomous UGV applications, such as logistics, cleaning, and patrol, in closed environments like the campus and park. It has exhibited its applicability in GNSS/INS integrated navigation, SLAM, and multi-sensor fusion navigation. Future works include further exploring the potential of the i2Nav-Robot dataset in large-scale mapping, as building a practical high-precision map

has already become a basic capability of commercial UGVs.

References

[1] R. Siegwart, I. R. Nourbakhsh, and D. Scaramuzza, *Introduction to autonomous mobile robots*, 2nd ed. in Intelligent robotics and autonomous agents. Cambridge, Mass: MIT Press, 2011.

[2] H. Tang, T. Zhang, X. Niu, J. Fan, and J. Liu, "Impact of the Earth Rotation Compensation on MEMS-IMU Preintegration of Factor Graph Optimization," *IEEE Sens. J.*, vol. 22, no. 17, pp. 17194–17204, Sept. 2022.

[3] T. Zhang, M. Yuan, L. Wang, H. Tang, and X. Niu, "A Robust and Efficient IMU Array/GNSS Data Fusion Algorithm," *IEEE Sens. J.*, vol. 24, no. 16, pp. 26278–26289, Aug. 2024.

[4] P. J. G. Teunissen and O. Montenbruck, Eds., *Springer Handbook of Global Navigation Satellite Systems*. Cham: Springer International Publishing, 2017.

[5] P. D. Groves, *Principles of GNSS, inertial, and multisensor integrated navigation systems*. Boston: Artech House, 2008.

[6] H. Tang, X. Niu, T. Zhang, Y. Li, and J. Liu, "OdoNet: Untethered Speed Aiding for Vehicle Navigation Without Hardware Wheeled Odometer," *IEEE Sens. J.*, vol. 22, no. 12, pp. 12197–12208, June 2022.

[7] Z. Zhang, X. Niu, H. Tang, Q. Chen, and T. Zhang, "GNSS/INS/ODO/wheel angle integrated navigation algorithm for an all-wheel steering robot," *Meas. Sci. Technol.*, vol. 32, no. 11, p. 115122, Nov. 2021.

[8] L. Wang, X. Niu, T. Zhang, H. Tang, and Q. Chen, "Accuracy and robustness of ODO/NHC measurement models for wheeled robot positioning," *Measurement*, vol. 201, p. 111720, Sept. 2022.

[9] L. Wang, H. Tang, T. Zhang, Y. Wang, Q. Zhang, and X. Niu, "PO-KF: A Pose-Only Representation-based Kalman Filter for Visual Inertial Odometry," *IEEE Internet Things J.*, pp. 1–20, 2025.

[10] H. Tang, T. Zhang, L. Wang, M. Yuan, and X. Niu, "BA-LINS: A Frame-to-Frame Bundle Adjustment for LiDAR-Inertial Navigation," *IEEE Trans. Intell. Transp. Syst.*, vol. 26, no. 5, pp. 6621–6634, May 2025.

[11] J. Yin, A. Li, T. Li, W. Yu, and D. Zou, "M2DGR: A Multi-Sensor and Multi-Scenario SLAM Dataset for Ground Robots," *IEEE Robot. Autom. Lett.*, vol. 7, no. 2, pp. 2266–2273, Apr. 2022.

[12] X. Shi *et al.*, "Are we ready for service robots? the openloris-scene datasets for lifelong slam," in *2020 IEEE international conference on robotics and automation (ICRA)*, IEEE, 2020, pp. 3139–3145.

[13] Y. Tian *et al.*, "Resilient and Distributed Multi-Robot Visual SLAM: Datasets, Experiments, and Lessons Learned," in *2023 IEEE/RSJ International Conference on Intelligent Robots and Systems (IROS)*, Oct. 2023, pp. 11027–11034.

[14] Y. Liu *et al.*, "BotanicGarden: A High-Quality Dataset for Robot Navigation in Unstructured Natural Environments," *IEEE Robot. Autom. Lett.*, vol. 9, no. 3, pp. 2798–2805, Mar. 2024.

[15] T. Pire, M. Mujica, J. Civera, and E. Kofman, "The Rosario dataset: Multisensor data for localization and mapping in agricultural environments," *Int. J. Robot. Res.*, vol. 38, no. 6, pp. 633–641, May 2019.

[16] D. Zhang *et al.*, "Towards Robust Sensor-Fusion Ground SLAM: A Comprehensive Benchmark and A Resilient Framework." arXiv, July 11, 2025.

[17] Y. Zhuang, B. Wang, J. Huai, and M. Li, "4D iRIOM: 4D Imaging Radar Inertial Odometry and Mapping," *IEEE Robot. Autom. Lett.*, vol. 8, no. 6, pp. 3246–3253, June 2023.

[18] Z. Yan, L. Sun, T. Krajník, and Y. Ruichek, "EU Long-term Dataset with Multiple Sensors for Autonomous Driving," in *2020 IEEE/RSJ International Conference on Intelligent Robots and Systems (IROS)*, 2020, pp. 10697–10704.

[19] J. Zhang *et al.*, "NTU4DRadLM: 4D Radar-Centric Multi-Modal Dataset for Localization and Mapping," in *2023 IEEE 26th International Conference on Intelligent Transportation Systems (ITSC)*, Sept. 2023, pp. 4291–4296.

[20] N. Carlevaris-Bianco, A. K. Ushani, and R. M. Eustice, "University of Michigan North Campus long-term vision and lidar dataset," *Int. J. Robot. Res.*, vol. 35, no. 9, pp. 1023–1035, 2016.

[21] J. Jiao *et al.*, "FusionPortable: A Multi-Sensor Campus-Scene Dataset for Evaluation of Localization and Mapping Accuracy on Diverse Platforms," in *2022 IEEE/RSJ International Conference on Intelligent Robots and Systems (IROS)*, Oct. 2022, pp. 3851–3856.

[22] H. Wei *et al.*, "FusionPortableV2: A unified multi-sensor dataset for generalized SLAM across diverse platforms and scalable environments," *Int. J. Robot. Res.*, p. 02783649241303525, Dec. 2024.

[23] H. Li *et al.*, "MARS-LVIG dataset: A multi-sensor aerial robots SLAM dataset for LiDAR-visual-inertial-GNSS fusion," *Int. J. Robot. Res.*, p. 02783649241227968, Jan. 2024.

[24] M. Burri *et al.*, "The EuRoC micro aerial vehicle datasets," *Int. J. Robot. Res.*, vol. 35, no. 10, pp. 1157–1163, Sept. 2016.

[25] A. Kaehler and G. Bradski, *Learning OpenCV 3: computer vision in C++ with the OpenCV library*. O'Reilly Media, Inc., 2016.

[26] E. Olson, "AprilTag: A robust and flexible visual fiducial system," in *2011 IEEE International Conference on Robotics and Automation*, May 2011, pp. 3400–3407.

[27] H. Tang, T. Zhang, X. Niu, L. Wang, L. Wei, and J. Liu, "FF-LINS: A Consistent Frame-to-Frame Solid-State-LiDAR-Inertial State Estimator," *IEEE Robot. Autom. Lett.*, vol. 8, no. 12, pp. 8525–8532, Dec. 2023.

[28] H. Tang, X. Niu, T. Zhang, L. Wang, and J. Liu, "LE-VINS: A Robust Solid-State-LiDAR-Enhanced Visual-Inertial Navigation System for Low-Speed Robots," *IEEE Trans. Instrum. Meas.*, vol. 72, pp. 1–13, 2023.

[29] T. Qin, P. Li, and S. Shen, "VINS-Mono: A Robust and Versatile Monocular Visual-Inertial State Estimator," *IEEE Trans. Robot.*, vol. 34, no. 4, pp. 1004–1020, Aug. 2018.

[30] P. Geneva, K. Eckenhoff, W. Lee, Y. Yang, and G. Huang, "OpenVINS: A Research Platform for Visual-Inertial Estimation," in *2020 IEEE International Conference on Robotics and Automation (ICRA)*, Paris, France: IEEE, May 2020, pp. 4666–4672.

[31] L. von Stumberg and D. Cremers, "DM-VIO: Delayed Marginalization Visual-Inertial Odometry," *IEEE Robot. Autom. Lett.*, vol. 7, no. 2, pp. 1408–1415, Apr. 2022.

[32] K. Chen, R. Nemiroff, and B. T. Lopez, "Direct LiDAR-Inertial Odometry: Lightweight LIO with Continuous-Time Motion Correction," in *2023 IEEE International Conference on Robotics and Automation (ICRA)*, May 2023, pp. 3983–3989.

[33] W. Xu, Y. Cai, D. He, J. Lin, and F. Zhang, "FAST-LIO2: Fast Direct LiDAR-Inertial Odometry," *IEEE Trans. Robot.*, pp. 1–21, 2022.

[34] C. Zheng *et al.*, "FAST-LIVO2: Fast, Direct LiDAR–Inertial–Visual Odometry," *IEEE Trans. Robot.*, vol. 41, pp. 326–346, 2025.

[35] J. Lin and F. Zhang, "R3LIVE: A Robust, Real-time, RGB-colored, LiDAR-Inertial-Visual tightly-coupled state Estimation and mapping package," in *2022 International Conference on Robotics and Automation (ICRA)*, 2022, pp. 10672–10678.

[36] M. Grupp, "evo." Mar. 2023. [Online]. Available: https://github.com/MichaelGrupp/evo

[37] i2Nav Group, "KF-GINS." in An EKF-Based GNSS/INS Integrated Navigation System. i2Nav-WHU, 2024. [Online]. Available: https://github.com/i2Nav-WHU/KF-GINS

[38] T. Qin, S. Cao, J. Pan, and S. Shen, "A General Optimization-based Framework for Global Pose Estimation with Multiple Sensors," *ArXiv190103642 Cs*, Jan. 2019. [Online]. Available: http://arxiv.org/abs/1901.03642

[39] X. Niu, H. Tang, T. Zhang, J. Fan, and J. Liu, "IC-GVINS: A Robust, Real-Time, INS-Centric GNSS-Visual-Inertial Navigation System," *IEEE Robot. Autom. Lett.*, vol. 8, no. 1, pp. 216–223, Jan. 2023.

[40] W. Lee, P. Geneva, C. Chen, and G. Huang, "MINS: Efficient and Robust Multisensor-Aided Inertial Navigation System," *J. Field Robot.*, May 2025.

[41] C. Chi, X. Zhang, J. Liu, Y. Sun, Z. Zhang, and X. Zhan, "GICI-LIB: A GNSS/INS/Camera Integrated Navigation Library," *IEEE Robot. Autom. Lett.*, vol. 8, no. 12, pp. 7970–7977, Dec. 2023.